Supplementary Figures

Related to Figure 1:

Figure S1: Effect of Hypo-osmotic Shock on Plasma Membrane and Caveolae Distribution.

Movie S1A: Dynamics of Caveolae in Control Cells

Movie S1B: Dynamics of Caveolae under Hypo-osmotic Shock

Related to Figure 3:

Figure S2: Electron Micrographs of Cav1 Labeling and Stereo Electron Micrographs of Flat and Budded Caveola Structures by Deep Etch EM.

Related to Figure 4:

Figure S3: Membrane Tether Pulling, Caveolae Distribution and Expression, and Analysis of Cortical Actin in Response to Hypo-osmotic Exposure in Live MLEC.

Figure S4: Single Cell Quantification of the Loss of Caveolae and Clathrin Structures upon Hypo-osmotic shock and Contribution to Membrane Tension Buffering.

Figure S5: Increased Susceptibility to Cell Membrane Rupturing upon Hypo-osmotic Shock in Cells where Caveolae Function is Impaired.

Movie S2: Movie of Tether Pulling

Related to Figure 5:

Movie S3A: Epifluorescence Movie of Intracellular Pool of Cav1-EGFP

Movie S3B: Effect of ATP Depletion on Caveola Mobility

Figure S6: Effect of CD Treatment and ATP Depletion on Caveolae Loss in Stretched Cells and in Membrane Tension Buffering During Hypo-osmotic Shock in MLEC.

Figure S7: Caveola Morphology After CD Treatment and ATP Depletion in wt MLEC.

Figure S8: Resting Membrane Tension Depends on the Presence of Caveolae, Actin Dynamics and Active Cellular Machinery.

Supplementary Figure S1 for Figure1

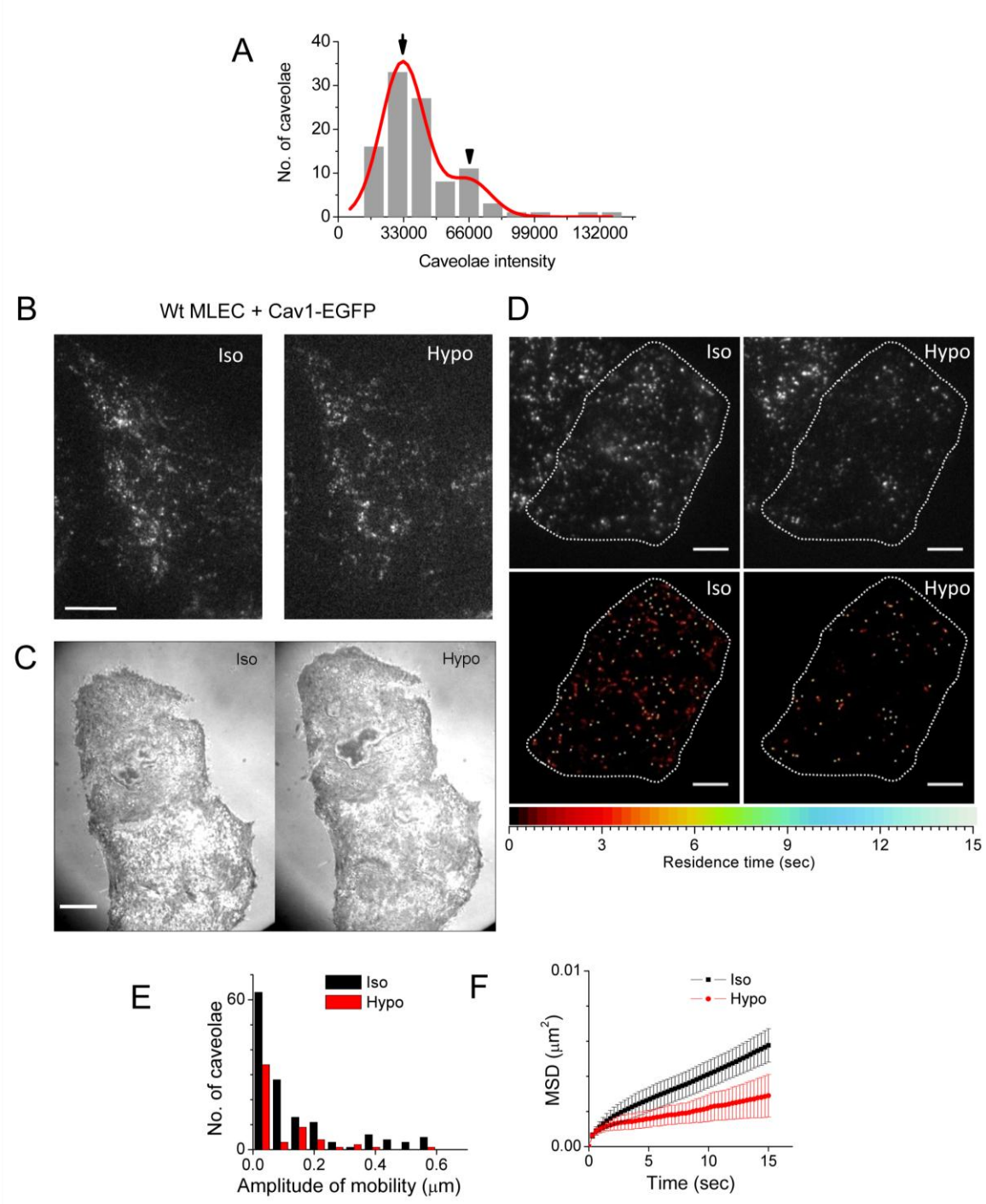

Figure S1: Effect of Hypo-osmotic Shock on Plasma Membrane and Caveolae Distribution.

(A) Caveolae detection was done by image analysis and it was checked for the characteristic quantal assembly of Cav1-EGFP in caveolae (Pelkmans and Zerial, 2005). Cav1-EGFP intensity per caveolae was calculated for individual punctuated structures (caveola) from TIRF images of Cav1-EGFP expressed in HeLa cells. Representative intensity distribution for all caveolae (n = 103) imaged in one cell shows two distinct intensity levels (peaks marked

out by arrows). The peak intensities increase by quantal size. The left peak represents the smallest quantum of Cav1-EGFP per caveola and and a second peak is found with twice the amount of Cav1-EGFP per caveolar structure (right arrow). The red line shows a Gaussian fit.

(B) Images depicting loss of caveolae after 5 min hypo-osmotic shock in wt MLECs transfected with Cav1-EGFP. The loss was measured to be 30%. Bar = 5 µm.

(C) RICM image of HeLa Cav1-EGFP cells before (Iso) and after hypo-osmotic shock of 5 min (Hypo). Upon hypo-osmotic shock, the proximity of the plasma membrane to the glass surface is increased (expansion of the central dark patch) ruling out the possibility of loss of contact between the plasma membrane and glass surface. Bar = 5 µm.

(D) Top: TIRF image of HeLa Cav1-EGFP cells in iso-osmotic conditions (Iso) and after hypo-osmotic shock (4 min) (Hypo). Bottom: Color coded image of residence time (sec) of centers of mass of caveolae before (Iso) and after (Hypo) hypo-osmotic shock (4 min) tracked over 15 seconds with a time interval of 300 ms. Dotted line marks out the cell footprint. Bar = 5 µm.

(E) Amplitude of caveolae mobility quantified by standard deviation of the caveolae position tracked for 15 sec with 300 ms time interval for the cell (shown in Figure S1D) before (Iso) and after (Hypo) hypo-osmotic shock.

(F) Average mean square displacement (MSD) of slow-moving caveolae in control (black,) and hypo-osmotic shocked cells (red). The mobility of slow moving caveolae is reduced after hypo-osmotic shock. Data represents mean ± standard deviations from > 300 caveolae tracks obtained from 5 cells imaged before and after hypo-osmotic shock.

Supplementary Figure S2 for Figure 3

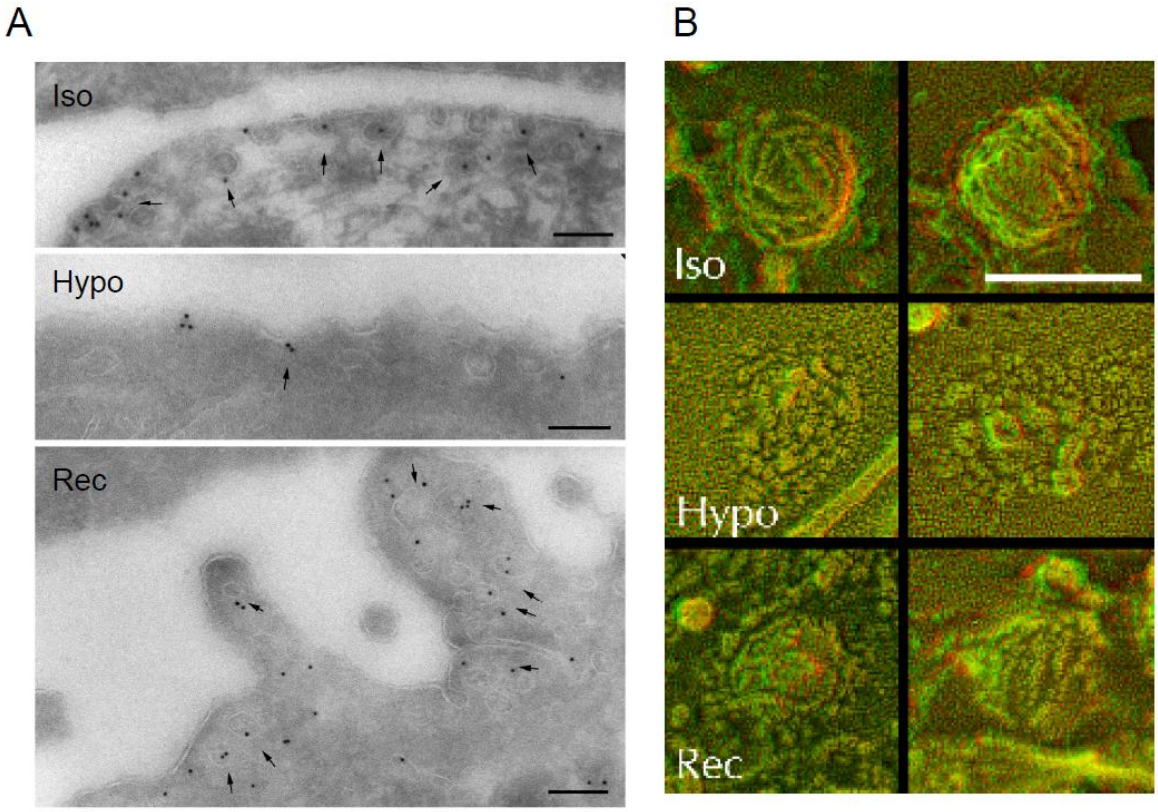

Figure S2: Electron Micrographs of Cav1 Labeling and Stereo Electron Micrographs of Flat and Budded Caveola Structures by Deep Etch EM.

(A) Immuno-EM images of ultrathin cryosections with gold-tagged Cav1 antibody of wt MLEC under iso-osmotic (Iso), hypo-osmotic (Hypo) and recovered iso-osmotic (Rec) conditions. Bar = 200 nm.

(B) EM anaglyph of wt MLEC under iso-osmotic (Iso), hypo-osmotic (Hypo) and recovered iso-osmotic (Rec) conditions imaged by deep etch electron microscopy. Using view glasses (left = red), the three dimensional form of budded and flat caveolar structures become visible. Bar = 100 nm.

Supplementary Figure S3 for Figure 4

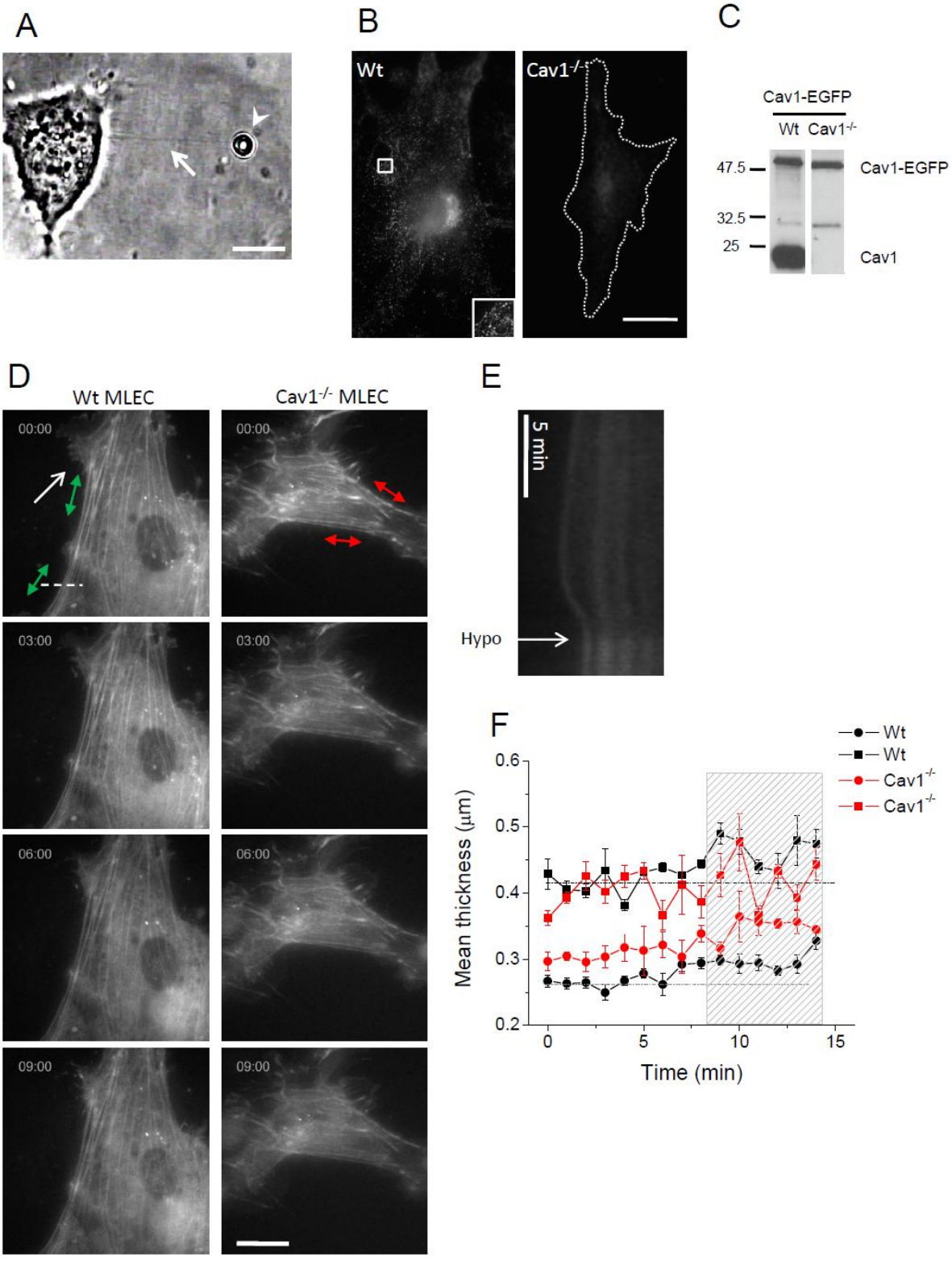

Figure S3: Membrane Tether Pulling, Caveolae Distribution and Expression, and Analysis of Cortical Actin in Response to Hypo-osmotic Exposure in Live MLEC.

(A) Representative bright field image of a tether (arrow) pulled from the plasma membrane of a Cav1$^{-/-}$ MLEC using an optically trapped bead (arrow head). Controlled movement of the stage enables to extract and lengthen the tether. The resulting displacement of the bead from the center of the optical trap is measured to compute the tether force.

(B) Cav1 expression in wt and Cav1$^{-/-}$ MLEC assayed by immunofluorescence. Cav1 is abundant in wt MLEC and is organized in small clusters predominantly at the plasma membrane (the inset shows a 2x magnification of the marked region), whereas it is absent in Cav1$^{-/-}$ MLEC. Dashed line marks out the cell boundary. Bar = 10 µm.

(C) Cav1 expression in wt and Cav1$^{-/-}$ MLEC transfected with Cav1-EGFP assayed by immunoblotting. Endogenous Cav1 (22-24 kDa) is present in wt, but not in Cav1$^{-/-}$ MLEC, whereas Cav1-EGFP (51 kDa) is expressed in both cell lines.

(D) Widefield fluorescence (using 1.45 NA, 100X objective) images of wt MLEC and Cav1$^{-/-}$ MLEC before (iso) and after various time intervals (in minutes) after hypo-osmotic shock (t=0 min, 150 mOsm). White arrow points to a lamellipodium. Dashed line shows the section for which the kymograph representation is presented in (E) Bar = 20 µm.

(E) Kymograph (representation of time versus spatial position) of the peripheral actin bundles in the section shown by the dashed line in (D). White arrow marks out t = 0. The immediate outward movement of actin bundles and late changes in intensity and thickness are qualitatively observed.

(F) Quantification of the peripheral actin bundle thickness of the regions marked out by double headed arrows in D, over time after hypo-osmotic shock (onset at t = 0). Top and bottom double headed arrows for wt and Cav1$^{-/-}$ MLEC (in left and right panels in A) are the corresponding regions used for the top (filled squares) and bottom (filled circles) traces. For each time point, first, multiple images (maximum 12, time binning 5 sec) were used and the cross-sectional intensity profile of the actin bundle closest to the plasma membrane were fit with Gaussian functions to derive the thickness. This was repeated for different positions in the same region (N = 4 for each region).

Supplementary Figure S4 for Figure 4

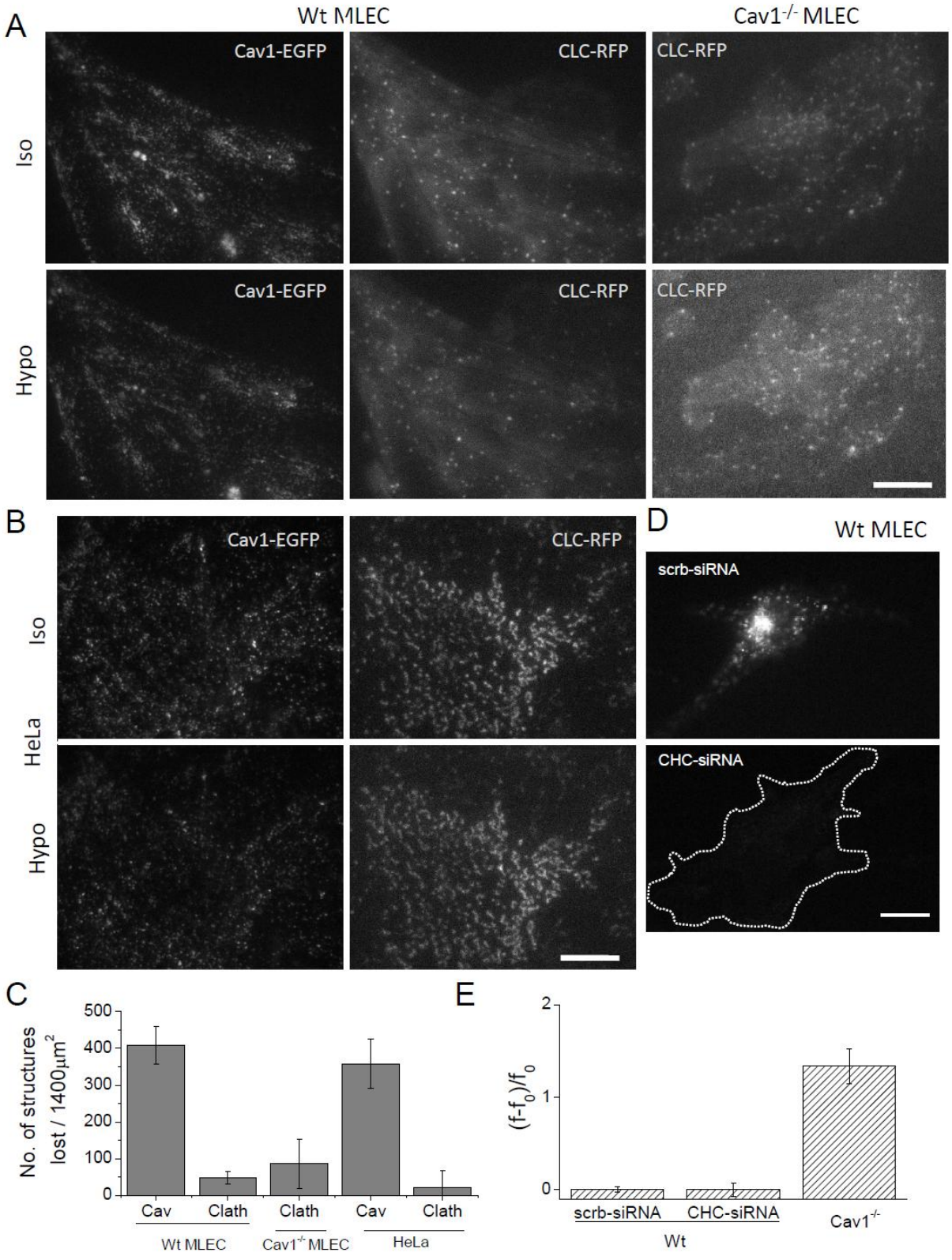

Figure S4: Single Cell Quantification of the Loss of Caveolae and Clathrin Structures upon Hypo-osmotic shock and Contribution to Membrane Tension Buffering.

(A) Wt MLEC transfected with Cav1-EGFP and Clathrin light chain RFP (CLC-RFP) and Cav1$^{-/-}$ MLEC transfected with CLC-RFP imaged in TIRF in iso-osmotic condition and 5 min after hypo-osmotic shock (30 mOsm). Bar = 10 µm.

(B) HeLa cells expressing Cav1-EGFP and CLC-RFP imaged by TIRF in iso-osmotic and hypo-osmotic conditions (5min, 30 mOsm). Bar = 10 µm.

(C) Quantification of the average number of lost caveolae and clathrin coated pits (in ~1400 µm^2 projected area of the cell) after hypo-osmotic shock in wt and Cav1$^{-/-}$ MLEC and HeLa cells. Data represents mean ± standard error. (N = 2 for MLEC, N = 4 for HeLa).

(D) Epifluorescence imaging of transferrin-Alexa594 endocytosis after 5 min of incubation in wt MLEC transfected with scrambled siRNA (scrb-siRNA, top) or clathrin heavy chain siRNA (CHC-siRNA, bottom). Cells with no transferrin uptake were considered as efficiently transfected with CHC-siRNA, and used for further tether extraction and hypo-shock experiments. Bar = 10 µm.

(E) Relative change of the tether force f after hypo-osmotic shock (5min) with respect to the force in iso-osmotic conditions f_0 in wt-MLEC transfected with scrambled siRNA (scrb-siRNA, N = 7) or clathrin heavy chain siRNA (CHC-siRNA, N = 9), and in Cav1$^{-/-}$ MLEC (N = 10, p = 3E-4) devoid of caveolae, but having clathrin-coated pits. Data represent mean ± standard errors.

Supplementary Figure S5 for Figure 4

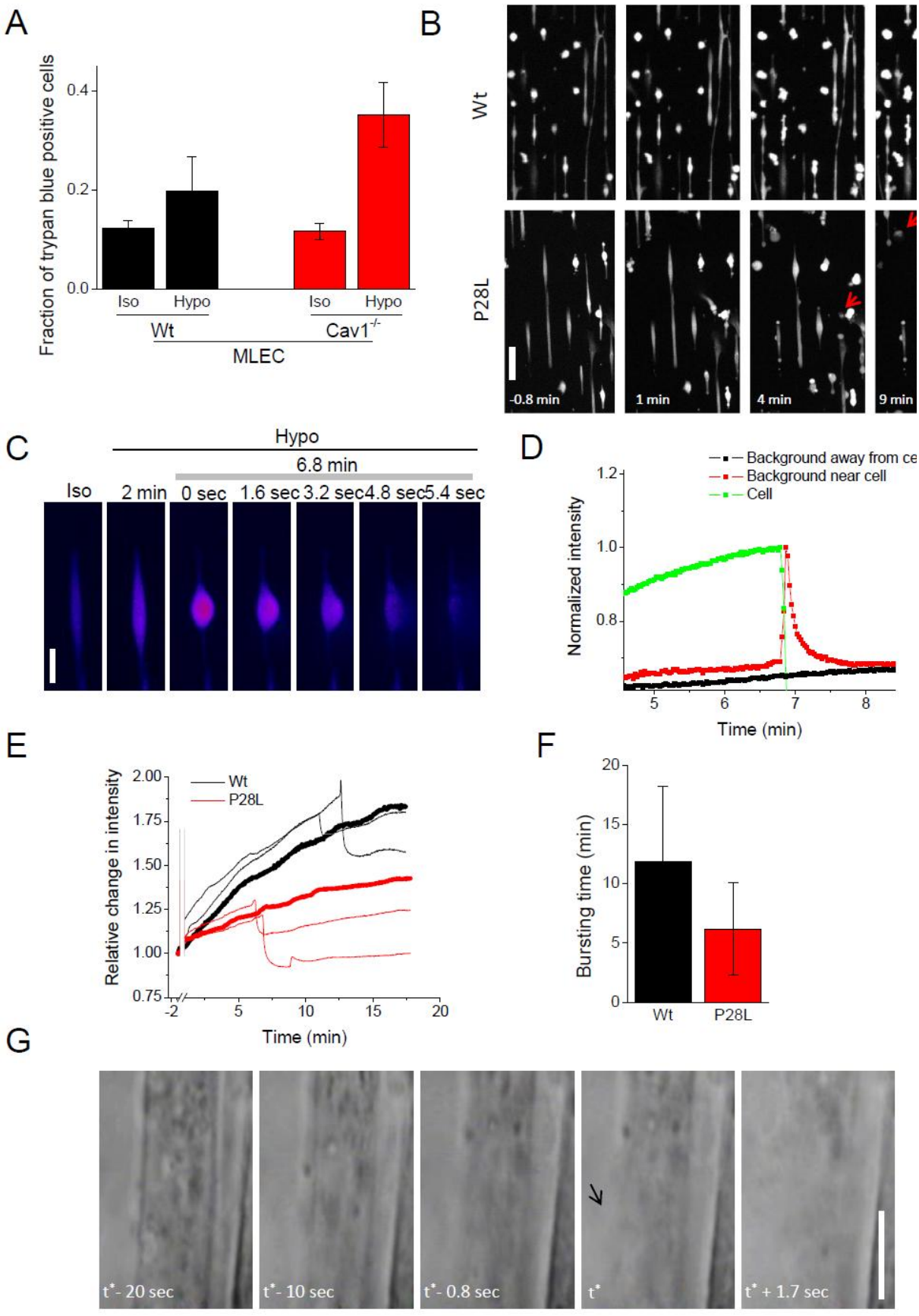

Figure S5. Increased Susceptibility to Cell Membrane Rupturing upon Hypo-osmotic Shock in Cells where Caveolae Function is Impaired.

(A) Wt and Cav1$^{-/-}$ MLEC under iso-osmotic condition or 5 min hypo-osmotic shock (30 mOsm) were detached and stained with Trypan blue. Data show the mean ± standard deviation of three independent experiments (N = 100 cells per experiment).

(B) Low-magnification epifluorescence snapshots of wt and P28L Cav3 mutant myotubes after hypo-osmotic shock (30mOsm, t = 0). Wt and P28L mutant myotubes were grown on patterned glass coverslips. Membrane rupture in response to hypo-osmotic shock was assessed using Calcein-AM, a cell permeable non fluorescent molecule that becomes fluorescent only in live cells and leaks out in case of membrane rupture. Fluorescence imaging at 5X magnification and 1.6 sec time binning was done to image ~200-300 cells before and during hypo-osmotic exposure in the continued presence of Calcein-AM. Representative images depict a higher frequency of bursting (events marked by red crosses) in P28L than wt myotubes. Bar = 100 µm.

(C) Images of a P28L myotube rupturing at t = 6.8 minutes after shock. Bar = 50 µm.

(D) Plot of fluorescence intensity in inside a bursting cell (green squares and line), in its close vicinity (red squares and line), and far away from the cell (black squares and line).

(E) Relative intensity increase in single myotubes that either burst (thin lines) or do not burst upon hypotonic exposure for 20 minutes (thick lines) at t = 17 minutes of imaging.

(F) Average bursting time of wt (N = 5) and Cav3-P28L (N = 7) myotubes. Error bars represent standard deviation.

(G) Bright-field high-magnification snapshots of a P28L myotube exposed to hypotonic shock and exhibiting membrane rupture. Images are shown just before and after bursting time, t^*, to highlight membrane permeabilization (loss of contrast) and subsequent loss of membrane integrity (black arrow). Bar = 5 µm.

t*

Supplementary Figure S6 for Figure 5

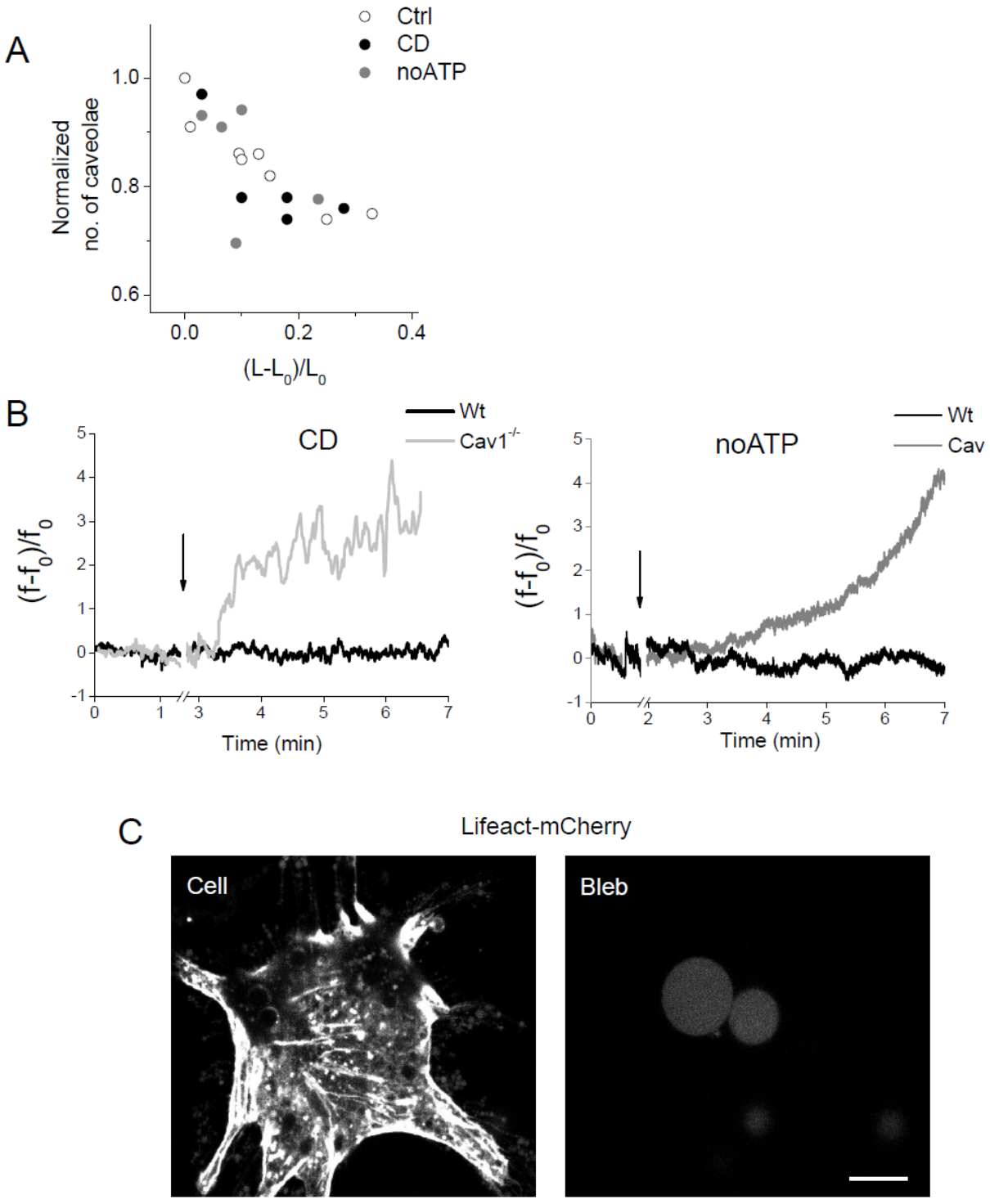

Figure S6: Effect of CD treatment and ATP depletion on Caveolae Loss in Stretched Cells and in Membrane Tension Buffering During Hypo-osmotic Shock in MLEC.

(A) Change in number of caveolae for single HeLa Cav1-EGFP cells stretched to different lengths in control (Ctrl), CD treated (CD) and ATP depleted (no ATP) cells. Each data point represents the loss for a particular cell. The loss of caveolae is correlated to the extent of stretch (Ctrl: N=7; CD: N = 5; no ATP: N = 5).

(B) Representative force curves for membrane tethers extracted from wt MLEC (black) and $Cav1^{-/-}$ MLEC (grey) treated with cytochalasin D (CD) or ATP depleted (no ATP) and exposed to hypo-osmotic shock. A membrane tether is first extracted in iso-osmotic conditions (0 min < t < ~1 min) and maintained at constant length during the whole course of the experiment. During medium dilution, the tether force is not recorded (break in the time axis). The arrow marks out the end of medium dilution (i.e. when osmolarity reaches 150 mOsm). The curve represents the relative change of the tether force f with respect to the initial force f_0. Whereas the magnitude of force increase in $cav1^{-/-}$ MLECs is conserved from one experiment to another, the kinetics of force increase is variable.

(C) Confocal images of wt MLEC transfected with Lifeact-mCherry to visualize the distribution of polymerizing actin after 6 hrs of incubation in PMS-buffer. Actin filaments are visible in the cell body (Cell) due to binding of Lifeact-mCherry, whereas only a faint diffused signal of the cytosolic Lifeact-mCherry is detectable in the blebs which are on the top of the cell (Bleb) shown in the left image. Bar = 10 μm.

Supplementary Figure S7 for Figure 5

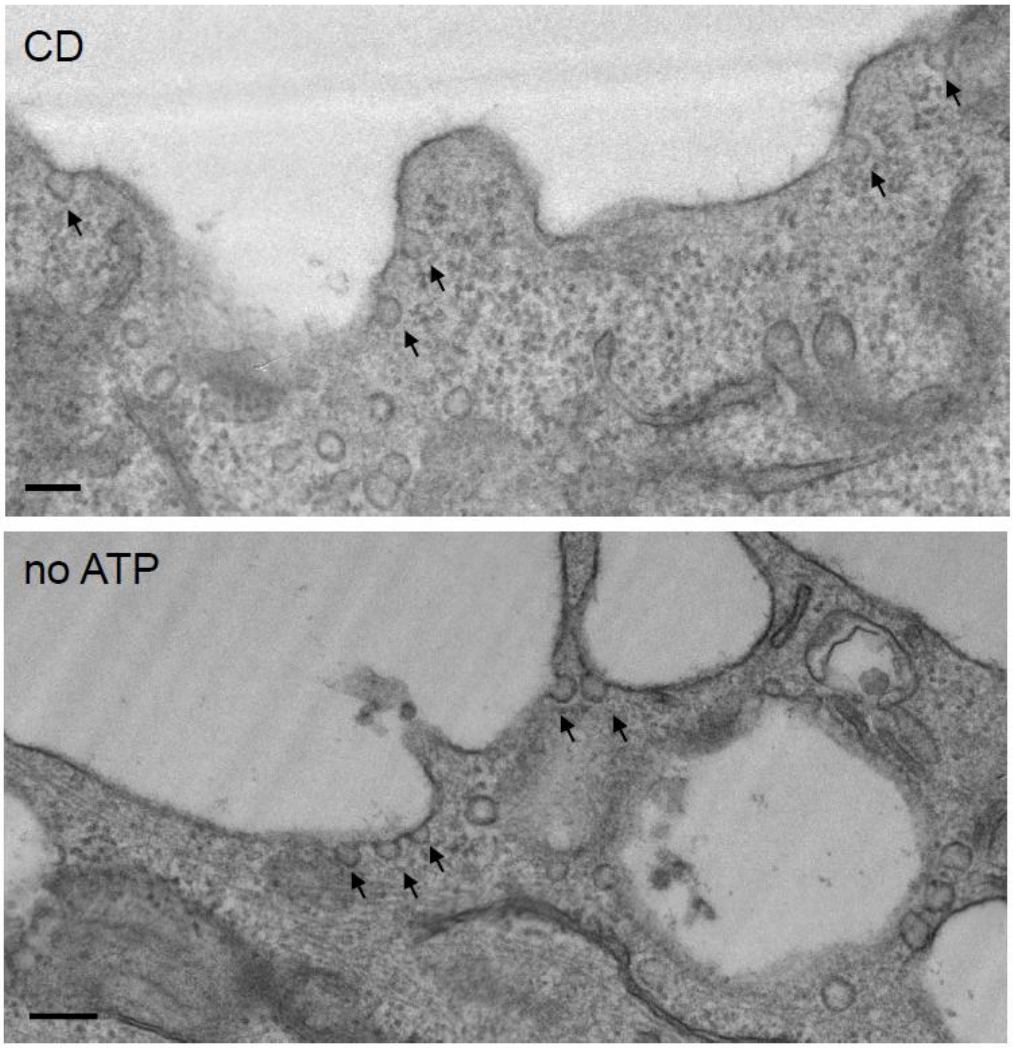

Figure S7: Caveola Morphology After CD Treatment and ATP depletion in wt MLEC. Ultrathin cryosections of cytochalasin D (CD) treated and ATP depleted (no ATP) wt MLEC examined by electron microscopy. Bar = 200nm.

Supplementary Figure S8

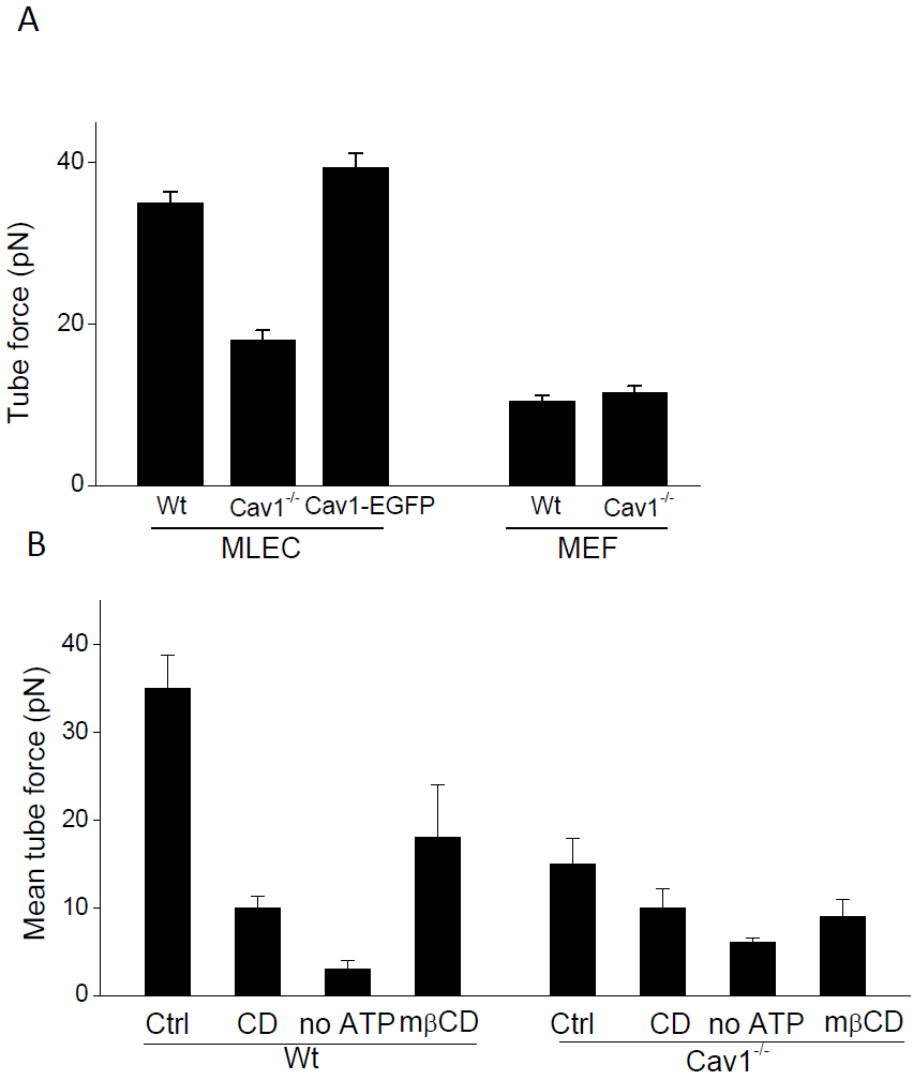

Figure S8: Resting Membrane Tension Depends on the Presence of Caveolae, Actin Dynamics and Active Cellular Machinery.

(A) Tether force in MLECs is significantly lower in Cav1$^{-/-}$ MLEC and can be restored to wt values by transfection of Cav1-EGFP. Tether forces exhibit no significant differences in wt and Cav1$^{-/-}$ MEF.

(B) Tether force measured in resting MLEC is decreased when actin dynamics are blocked with cytochalasin D (CD), upon ATP depletion (no ATP) or caveola flattening with mβCD treatment.